Colloids and Surfaces A: Physicochemical and Engineering Aspects 682 (2024) 132942

Contents lists available at ScienceDirect

Colloids and Surfaces A: Physicochemical and Engineering Aspects

journal homepage: www.elsevier.com/locate/colsurfa

Particle-wall hydrodynamic effects on optical trapping viscometry

Richa Ghosh [a], Sarah A. Bentil [a,*], Jaime J. Juárez [a,b,**]

[a] Department of Mechanical Engineering, Iowa State University, Ames, Iowa 50011, USA
[b] Center for Multiphase Flow Research and Education, Iowa State University, Ames, Iowa 50011, USA

GRAPHICAL ABSTRACT

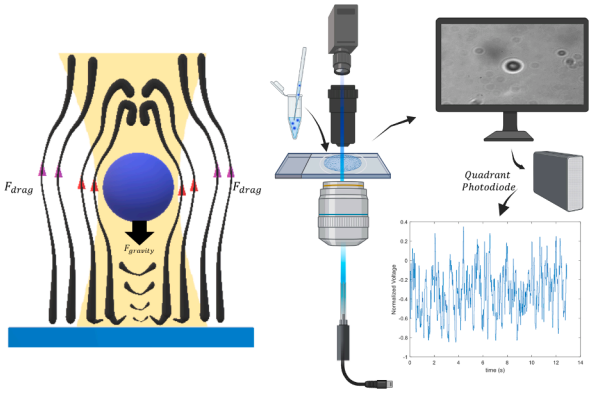

ARTICLE INFO

Keywords:
Optical tweezers
Viscometry
Hydrodynamic interactions
Brownian dynamics

ABSTRACT

Optical tweezers are a versatile setup used to measure forces in soft materials and characterize the rheological properties of fluids and gels. An accurate measurement of these forces is complicated by the interaction between the optically trapped materials and nearby substrate walls. This work presents a comprehensive Brownian Dynamic (BD) model that accounts for the hydrodynamic interactions between an optically trapped particle and a nearby boundary. The model is based on a midpoint algorithm, which simplifies accounting for diffusion gradients that arise from hydrodynamic interactions. Experiments using an optical tweezer and a quadrant position detector (QPD) are performed to validate these experiments. We conduct experiments by varying input laser current from 100 mA to 300 mA. Our experiments show that measured viscosity at 100 mA is ~19% higher than the value expected for room temperature water (0.89 mPa-s). The discrepancy diminishes to 4% when a 300 mA current is used. Simulations performed with the BD model show that, for a nominal spring constant of $k_s = 4.332 \times 10^{-4} I_{laser}$ $[pN/\mu m]$, the discrepancy can be explained via hydrodynamic interactions that influence the measured effective viscosity. Wide variability in confidence interactions observed in our data can be replicated by using a range of diameters in our simulation. This is consistent with DLS measurements of the particles used in this study, which show that the mean diameter was (1.63 ± 0.28) μm. This work has implications for measuring Newtonian media viscosities up to ~63 mPa-s, as determined by a scaling analysis of limitations for our measurement system.

* Corresponding author.
** Corresponding author at: Department of Mechanical Engineering, Iowa State University, Ames, Iowa 50011, USA.
E-mail addresses: sbentil@iastate.edu (S.A. Bentil), jjuarez@iastate.edu (J.J. Juárez).

https://doi.org/10.1016/j.colsurfa.2023.132942
Received 27 October 2023; Received in revised form 27 November 2023; Accepted 5 December 2023
Available online 7 December 2023

1. Introduction

Optical tweezers utilize optical gradient forces to trap and confine a variety of microscopic objects (e.g., cells, DNA, colloids) [1]. Direct applications of optical tweezers include the use of optical gradients to actively sort cells [2], guide the motion of micro-robots [3], and direct the assembly of colloidal particles into complex structures [4]. Using optical tweezers for these applications requires a fundamental understanding of the forces acting on particles at this scale [5]. For single particles in solution, these forces typically involve the relative contribution of optical gradient forces and viscous dissipation (i.e., hydrodynamic drag) [6]. This suggests that an accurate measurement of medium viscosity is required to fundamentally understand the dynamics of optically trapped particles.

The measurement of purely viscous samples using optically trapped particles is known as optical trapping viscometry. In this technique, the position of the optically trapped particle is measured using either high-speed video microscopy [7] or a quadrant position detector (QPD) [8]. The data collected from this measurement is typically analyzed using a power spectral density (PSD) to infer the diffusion coefficient of the particle, from which viscosity is obtained. While this technique provides an accurate measurement of diffusion coefficient, the measure value is dependent on local conditions due to hydrodynamic interactions between the optically trapped particle and nearby solid boundaries [9,10]. Directly calculating viscosity from measured data without correcting for hydrodynamic interactions will lead to measured viscosities deviating from expected values.

Accounting for hydrodynamic effects on optically trapped particles utilize a correction derived from the Navier-Stokes equations for a particle moving near a wall in a quiescent fluid (i.e., creeping flow) [11]. These models of hydrodynamic coupling are often used to interpret the measured dynamics of optically trapped particles but are rarely used to make dynamical predictions. The dynamical motion of optically trapped particles may be simulated using Brownian Dynamics (BD) [12–15], although the available models do not incorporate particle-wall hydrodynamics. When hydrodynamics are incorporated into models of optical trapping, they are intended to model the complex motion of a non-spherical particle [16,17] or hydrodynamic coupling between particle pairs [18]. Thus, given the ubiquity of hydrodynamic corrections for boundary effects in the optical trapping literature [19–23], there is a need to develop a comprehensive dynamic model for predicting these boundary effects.

The aim of this work is to develop a comprehensive BD simulation approach to characterizing hydrodynamic interactions between an optically trapped particle and a nearby substrate or boundary. The fundamental understanding gained from this model can aid the analysis of optical tweezer data for a variety of microscale systems. For example, optical tweezer measurements have shown that hydrodynamics have an impact on rheology of biological fluids, such as cytoplasm [24,25]. The measurement of colloidal diffusion at fluid interfaces [23] and in microfluidic devices [22] using optical trapping has exhibited an enhancement to drag as a result of hydrodynamic interactions, which is predicted by the BD model presented here. Although not the focus of this work, our model could be adjusted to yield insight into use of optical traps for measuring the hydrodynamically hindered kinetics of surfactant [26] and polymer [27] molecules at interfaces. Hence, the BD model presented here serves as a foundation from which to understand the impact that hydrodynamics has on a variety of optical trapping measurements.

Specifically, the article presents a BD model that accounts for the hydrodynamic interactions between an optically trapped particle and a nearby flat wall. This model uses a midpoint algorithm to integrate the Langevin equation and account for a diffusion coefficient that varies with height due to hydrodynamic interactions. This model is validated with optical trapping experiments where particle position is tracked using a QPD. The data is used to simultaneously calculate trap stiffness and effective medium viscosity. For our optical trapping system, we find that trap stiffness varies from 5.1×10^{-2} pN/μm to 1.33×10^{-1} pN/μm for an input laser current that ranges from 100 mA to 300 mA. The ensemble averaged medium viscosity obtained through experiment are up to 19% higher than the value expected for the medium at room temperature. Our BD simulations show that this result is consistent with the impact that hydrodynamic interactions have on the observed dynamics of the trapped particle. This work has implications for interpreting optical trapping viscometry measurements in Newtonian media.

2. Materials and methods

2.1. Sample preparation

Samples were sourced from commercially available silica particles (Spherotech, Cat No. SIP-15–10) with a nominal diameter of 1.56 μm. A silica particle dispersion was prepared by diluting the commercial stock with deionized (DI) water. This was done by taking 1 μL of silica particle stock and adding this volume to 99 μL of DI water in a micro-centrifuge tube (Fisherbrand, Cat No. 05–408–129). The dispersion was stored in a refrigerator at 4 °C for up to a week prior to use. The concentration of silica particles produced by this procedure was such that a single particle was observed in a typical video frame (1920 ×1200 pixels). The sample was mixed using a vortex mixer (INTLLAB, VM-370) before 10 μL of the dispersion was taken and placed on cover glass (VWR, 24 ×60 mm), Cat. No. 16004–096. The sample was sealed using a cover slip (22 ×22 mm, VWR coverslips, Cat. No. VWR #48366–227) with double-sided tape (Scotch, Permanent Double-Sided Tape, 3 M, 1/2inch, Cat. 137DM-2) acting as a spacer.

2.2. Optical tweezer system

The optical tweezer system is based on a platform available from Thorlabs (Cat. No. OTKB) mounted to an optical table. The system is used for optical trapping and is schematically shown in Fig. 1. Optical trapping is performed using a 976 nm infrared laser diode controlled by a compact laser diode drive (Thorlabs, Cat. No. CLD1015). Beam steering of the laser is achieved using a series of mirrors and dichroic filters. The beam is focused onto a particle using a 100 × Nikon E Plan MRP71900 (1.25NA, immersion oil) objective lens. This same lens is

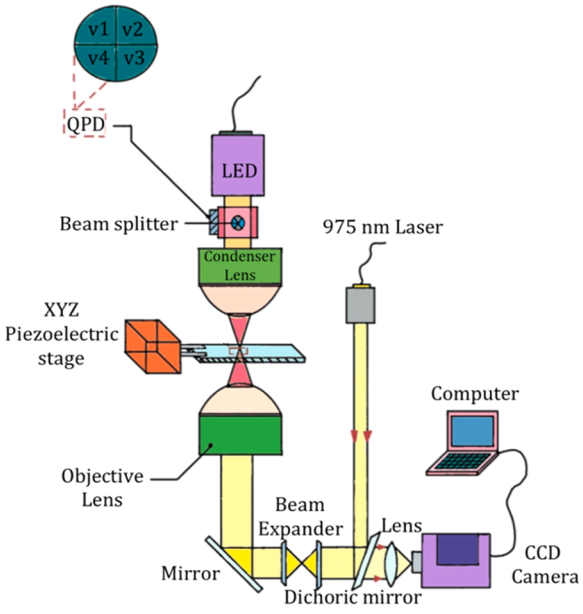

Fig. 1. A schematic diagram of the optical trapping system described in the work.

also used to observe particle trapping process with the aid of a CCD camera (Flir, Cat. No. BFLY-PGE-23S6M-C) recording at a rate of ~30 Hz. Samples are mounted to a three-axis piezoelectric translational stage (ThorLabs, Cat. No. NanoMax 300 TBB0606) that performs the microscale adjustments necessary to trap particles. A condenser stage consisting of an LED light and 10x/0.25 NA Nikon E Plan MRP70100 situated 7 mm above the sample is used to illuminate the stage during experiments. All experiments described in this work were performed at a temperature of 25 °C. Sample heating was minimized by using a low-power LED light for illumination and keeping output laser power below 100 mW, where the available literature has reported significant heating effects [28]. We measured a maximum power of 2.9 mW at the focusing objective lens using a power meter (Thorlabs, Cat.No. PM16–130).

The light scattered by the trapped particle is reflected by dichroic mirror into a QPD (ThorLabs, Cat. No. PDQ80A). The QPD recorded the position coordinates of the trapped particle in two dimensions by accounting for axial and lateral displacements from equilibrium. In our experiments, we modulated the laser power by changing the input current. At each of the laser currents characterized in this work, we performed 10 experiments. Each experiment consisted of 10,000 data points captured on the QPD at a rate of ~1 kHz. The data from the QPD was transmitted to a positioning detector (Thorlabs, Cat. No. KPA101) and stored on a text file with the aid of a code written in Python [29]. This data was analyzed using a code written MATLAB. The analysis process is described in the next section.

2.3. Data analysis

The positioning detector registers the observed location of the particle-deflected beam as the weighted average of voltage output, v, from four photodiodes. These weighted averages are,

$$x_n = \frac{(v_2 + v_3) - (v_1 + v_4)}{v_1 + v_2 + v_3 + v_4}$$

$$y_n = \frac{(v_1 + v_2) - (v_3 + v_4)}{v_1 + v_2 + v_3 + v_4}$$

where x_n and y_n are dimensionless positions as detected by the QPD. The properties of non-dimensional trajectories (e.g., decay time, diffusion coefficient, spring constant), are compared to simulated trajectories based on the model described in Section 3. Iterating through different conversion factors, we found that the best fit to our experimental data occurred when a conversion factor of β = 3.028 μm/A.U. was applied. This factor could then be applied to our dimensionless positions to obtain the position of the particle in dimensional units (i.e., $x = \beta x_n$ and. $y = \beta y_n$). The conversion factor found by this method is comparable to conversion factors reported in the literature for the same optical trapping system [30]. A discussion on how we arrived at this value of β for our data may be found in Supplementary Information.

The conversion factor is applied to the normalized position data to obtain dimensional position data. The dimensional position data is then used to determine the corner frequency observed in experiment by calculating the normalized autocorrelation function (NACF) [31],

$\frac{\langle r(0)r(t)\rangle}{\langle r(0)\rangle^2} = \exp(-\tau/\tau_c)$where r is position (either x or y), τ_c is a characteristic decay time, and τ is lag time. The term, $\langle r(0)\rangle^2$, represents the variance of position. At this point, the spring constant and effective medium viscosity can be determined in one of two ways. In the first approach, the equipartition method may be used to calculate the spring constant [32],

$k_s = \frac{k_B T}{\langle r(0)\rangle^2}$where k_B is Boltzmann's constant and T is ambient temperature. The effective viscosity of the medium can then be calculated using the decay time,

$\mu_{eff} = \frac{k_s \tau_c}{3\pi D}$where D is the trapped particle diameter. We refer to this term as an effective viscosity because the magnitude of this term is influenced by particle-wall hydrodynamic interactions. We discuss the details of this effect in the Theory section of our paper.

An alternative approach to determining system properties begins with the PSD. In this approach, a Fourier transform is applied to the position data to find the double-sided power spectrum [33]. The resulting power spectrum curve is fit to a Lorentzian curve of the form,

$P(f) = \frac{k_B T}{2\gamma\pi^2(f^2 + f_c^2)}$where $\gamma = 3\pi\mu_{eff}D$ is the Stokes drag coefficient, f is the spectrum frequency, and $f_c = 1/2\pi\tau_c$ is the corner frequency. The fitting process may be performed either by using γ and f_c as free parameters or by fixing the value of f_c based on the NACF procedure. The spring constant and effective viscosity may be calculated from these parameters,

$$k_s = 2\pi f_c \gamma$$

$$\mu_{eff} = \frac{\gamma}{3\pi D}$$

Our analysis of the data, implemented in MATLAB, utilized a blended approach whereby the spring constant and effective viscosity are calculated using both the NACF and PSD analyses. This approach showed that both analyses yielded similar values for k_s and μ_{eff}. All values reported for the experimental aspect of this work are based on the PSD analysis of the data using NACF to calculate the corner frequency. A schematic diagram of the data analysis workflow may be found in Supplemental Information.

3. Theory

The equation of motion for a colloidal particle in a viscous Newtonian medium can be modeled using the Langevin equation,

$$m\frac{d\boldsymbol{U}}{dt} = -\boldsymbol{F}_{drag} + \boldsymbol{F}_C + \boldsymbol{F}_B \quad (1)$$

Where m is the colloidal particle mass, $\boldsymbol{U}$ is the particle velocity vector, t is time, $\boldsymbol{F}_{drag}$ is the viscous drag force experienced by the particle, $\boldsymbol{F}_C$ is the net conservative force acting the particle, and $\boldsymbol{F}_B$ is Brownian force term. Fig. 2 schematically shows how the different force components contribute to the dynamics of an optically trapped particle. Specific force contributions are discussed below.

The drag force for a particle diffusing near a solid boundary in a quiescent fluid is expressed as [11],

$$\boldsymbol{F}_{drag} = 3\pi\mu_o D\boldsymbol{f}\boldsymbol{U} \quad (2)$$

where μ_o is the solvent viscosity and $\boldsymbol{f}$ is the friction factor associated with hydrodynamic interactions between the particle and nearby solid boundaries. Within this framework, the effective viscosity that would be measured in an optical trapping experiment is $\mu_{eff} = \mu_o\langle f\rangle$, where $\langle f\rangle$ is the ensemble-averaged friction factor experienced by a trapped particle during an experiment. The friction factors are directionally dependent on particle distance from the boundary. If the particle is diffusing parallel to the boundary (i.e., in the x or y axis) [34],

$$f_{\parallel} = \frac{12420\alpha^2 + 12233\alpha + 431}{12420\alpha^2 + 5654\alpha + 100} \quad (3)$$

where $\alpha = 2z/D - 1$, with z being the vertical distance from the boundary to the particle center (Fig. 2). When the particle moves in a direction normal to the solid boundary, the friction factor is [35],

$$f_{\perp} = \frac{6\alpha^2 + 9\alpha + 2}{6\alpha^2 + 2\alpha} \quad (4)$$

Eqs. 3 and 4 represent curve fits to the exact expressions [36] for these friction factors with a relative error of ± 0.001. We note that the expressions used in references [34,35] are inverted compared to what is presented here. This is because the authors of those references were interested in characterizing particle mobility, which is the inverse of

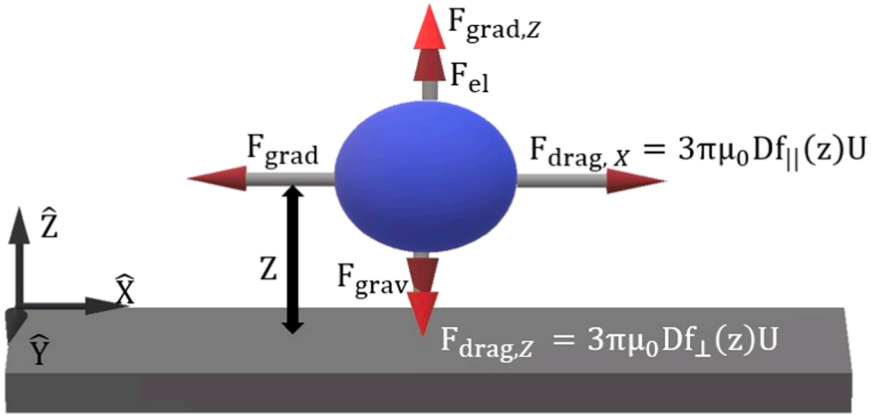

Fig. 2. A schematic diagram of a colloidal particle trapped by optical tweezers near a solid boundary.

particle drag, whereas we are interested in understanding the impact these friction factors have on particle drag.

The conservative force term represents the net effect of all non-dissipative forces acting on the particle. For this system, we consider the effect of the following forces,

$$\boldsymbol{F}_C = \boldsymbol{F}_{grav} + \boldsymbol{F}_{el} + \boldsymbol{F}_{grad} \tag{5}$$

where $\boldsymbol{F}_{grav}$ is the effect of gravity on the particle, $\boldsymbol{F}_{el}$ is the electrostatic interaction between the particle and the boundary, and $\boldsymbol{F}_{grad}$ represents the gradient force experienced by the particle trapped by the optical tweezers. The gravitational force acting on the particle is,

$$\boldsymbol{F}_{grav} = -\frac{\pi D^3}{6}(\rho_p - \rho_f)g \quad \hat{z} \tag{6}$$

Where ρ_p is the particle density, ρ_f is the fluid density, g is gravitational acceleration, and the caret hat operator (ˆ) indicates a unit vector pointing in the positive z-direction. The electrostatic force is modeled on Derjaguin's approximation for electrostatic interactions between a sphere and a plate [37],

$$\boldsymbol{F}_{el} = \kappa B_{pw} \exp[-\kappa(z-a)]\,\hat{z} \tag{7a}$$

where κ^{-1} is the Debye length and B_{pw} is,

$$B_{pw} = 8\varepsilon_m D\left(\frac{k_B T}{e}\right)^2 \tanh\left(\frac{e\psi_1}{4k_B T}\right)\tanh\left(\frac{e\psi_2}{4k_B T}\right) \tag{7b}$$

where ε_m is the dielectric permittivity of the medium, e is the charge of an electron, ψ_1 and ψ_2 are the Stern potentials of the sphere and the boundary, respectively. The gradient force in the normal direction due to the laser is [38],

$$\boldsymbol{F}_{grad,z} = -k_s \Delta z\left[1 + \left(\frac{\Delta z}{z_s}\right)^2\right]^{-2} \exp\left(-\left(\frac{\Delta z}{z_s}\right)^4\right)\hat{z} \tag{8a}$$

where $\Delta z = z - z_o$. The parameter, z_o, is the center of the optical trap in the vertical direction and $z_s = \pi\omega_o^2/\lambda_o$ is a distance parameter with ω_o being the beam waist diameter and λ_o being the laser wavelength. For the experimental system used in this work, $\omega_o = 1$ μm and $\lambda_o = 976$ nm, which corresponds to $z_s = 3.22$ μm. Our simulations suggest that our system is best modeled when z_o is a function of laser current, I_{laser}. The best fit to our data is achieved when,

$$\frac{z_o}{\mu m} = 13.6 - \frac{1966.9}{I_{laser}} + \frac{95666.5}{I_{laser}^2} \tag{8b}$$

Supplemental Information contains a discussion of how we arrived at this expression.

The laser force gradient in the axial direction, parallel to the boundary, is approximated as a Hookean spring,

$$\begin{aligned} \boldsymbol{F}_{grad,x} &= -k_s x \quad \hat{x} \\ \boldsymbol{F}_{grad,y} &= -k_s y \quad \hat{y} \end{aligned} \tag{9 -10}$$

We assume in our model that the spring constant is isotropic in the axial direction. Furthermore, we also assume that the particle begins its trajectory at the center of the optical trap. Thus, we do not consider field nonlinearity in the axial direction. However, we consider the nonlinear field component in the vertical direction since we do not know the equilibrium height beforehand. This height component is critical to correctly modeling the friction factors that arise from hydrodynamic interactions.

The Brownian force term fluctuates with a mean value of zero and is uncorrelated with time. It is modeled as [39],

$$\boldsymbol{F}_B = \boldsymbol{\xi}\sqrt{\frac{6\pi\mu_o D f k_b T}{\Delta t}} \tag{11}$$

where ξ is a three-term random vector drawn from a Gaussian distribution with a mean of zero and variance of one, while Δt is the simulation time step.

The challenge with directly integrating Eq. 1 using the model presented by Eqs. 2–11 is that the height dependence of the friction factor can lead to erroneously large steps, which impedes the proper reconstruction of the particle dynamics [40]. To compensate for the complexity of hydrodynamic interactions, we utilize the midpoint algorithm suggested by Fixman [41] to integrate Eq. 1. In this integration scheme, we assume that viscous drag dominates the inertial term of Eq. 1. Thus, the Langevin equation can be numerically integrated,

$$\boldsymbol{X}^s = \boldsymbol{X}^n + \frac{\Delta t}{2\gamma_o \boldsymbol{f}^n}\left[\boldsymbol{F}_C^n + \boldsymbol{F}_B^n\right] \tag{12}$$

The midpoint algorithm beings with the evaluation of a fractional step where $\gamma_o = 3\pi\mu_o D$ is the Stokes drag coefficient, $\boldsymbol{X}$ is a vector that contains the three-dimensional position of the particle, n is a time step index, and the index, s, represents variable evaluated at the fractional step.

All position dependent parameters ($\boldsymbol{f}$, $\boldsymbol{F}_c$, and $\boldsymbol{F}_B$) in this integration scheme are initially evaluated at position $\boldsymbol{X}^n$. After evaluating Eq. 12, the position of the fractional step, $\boldsymbol{X}^s$, is then used to update the friction factors, $\boldsymbol{f}^s = \boldsymbol{f}(\boldsymbol{X}^s)$, and conservative forces, $\boldsymbol{F}_C^s = \boldsymbol{F}_C(\boldsymbol{X}^s)$. Crucially, the Brownian force terms, $\boldsymbol{F}_B^n$, are not updated in this scheme [40]. The new friction factors and conservative forces are used to calculate the next positional step,

$$\boldsymbol{X}^{n+1} = \boldsymbol{X}^{n} + \frac{\Delta t}{\gamma_o f^s}\left[\boldsymbol{F}_C^s + \boldsymbol{F}_B^n\right] \tag{13}$$

The numerical scheme described by this section was coded in MATLAB and used to simulate 100 unique particles for 10^5 steps with a time step of 1 ms. The data was then processed using the same procedures we used to analyze our experimental results. The simulation data was compared to our experimental results as discussed below. A copy of the simulation code can be found in the Supplemental Information.

4. Results

We performed optical trapping experiments in water using a silica bead with a manufacturer reported 1.56 μm diameter. The experimental data was obtained at five different input currents from 100 mA to 300 mA. Each experiment was performed 10 times with different particles. Following the analysis procedure described in Section 2C, we initially processed the data to find the characteristic decay time of the NACF from which we determined the corner frequency ($f_c = 1/2\pi\tau_c$). Fig. 3 shows how our experimentally determined corner frequency varies as a function of laser current. The confidence intervals (CI) for the three lowest current settings are small, indicating that the true mean corner frequency lies within the error bars with 95% confidence. However, we observe that the input currents of 250 mA and 300 mA exhibit significantly larger CIs, indicating a larger variation in mean corner frequency obtained by experiment. A simulation performed using our midpoint algorithm model from Section 3 was performed using a 1.56 μm as an input diameter. While the simulation for the 1.56 μm particle follows the linear trend of the experimental data as a function of laser current, it does not explain the wide variability observed at higher input currents.

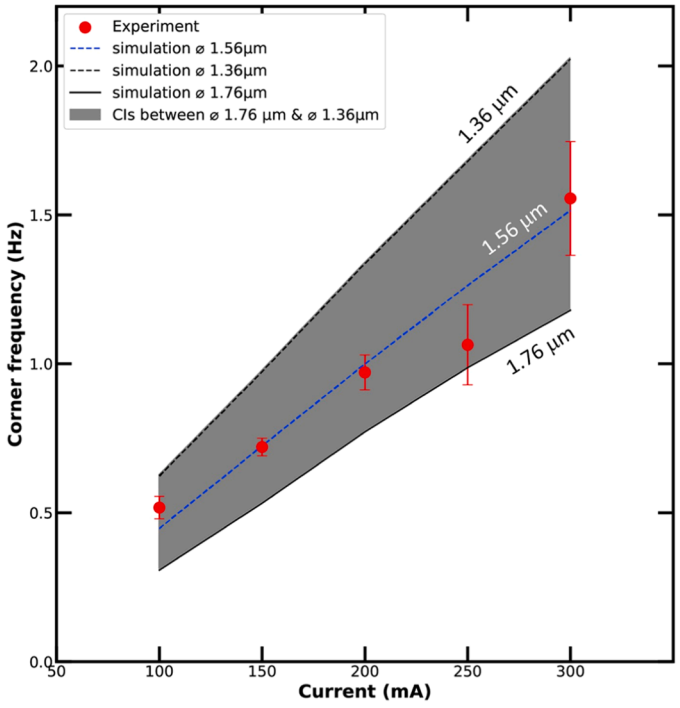

Fig. 3. Data (circles) collected from the ensemble-averaged corner frequency for optically trapped particles measured as a function of laser current. Experimental error bars represent 95% CI for N = 10 experiments. Lines show the ensemble-averaged results from 10^5 realizations of 100 simulated particle trajectories for three different particle diameters.

In order to determine the cause of these larger CIs, we consider an alternate definition of the corner frequency [42], $f_c = k_s/6\pi^2 D\mu_o\langle f\rangle$, where $\langle f\rangle$ represents the ensemble averaged friction factor. We note that the product, $\mu_o\langle f\rangle$, represents the effective viscosity that would be measured in an experiment. Thus, corner frequency is susceptible to errors or fluctuations in spring constant, particle diameter and drag correction factor. The spring constant is also dependent on several factors [43], $k_s \approx 2Q_r n_1 P/Dc$, where Q_r is the trapping efficiency, n_1 is the medium index of refraction, P is laser power, and c is the speed of light. The trapping efficiency is a difficult metric to determine due to variable transmission losses in the microscope objective and the optical path [44]. If we examine other parameters, we note that the index of refraction ($n_1 = 1.33$ for water) and the speed of light are well characterized, which means that we expect minimal contribution to the measured variability. The laser diode control module has a manufacturer reported current accuracy of ± (0.12% + 800 μA) and resolution of 100 μA [45]. Based on this reported accuracy, the current may vary from 300.4 mA to 301.2 mA during a typical experiment. Given that laser power is linearly proportional to current, we expect the variation in laser power to be similarly small.

We turn our attention to the particles used in these experiments, which were sourced from a commercial vendor. Dynamic light scattering (DLS) experiments found that the particles had a diameter of (1.63 ± 0.28) μm. This result represents a variation of ~17% between different particles drawn from the same source. The diameter influences the drag coefficient, γ_o, and it has an impact on the equilibrium position of the particle, which impacts $\langle f\rangle$. Based on our analysis in Supplemental Information, the most probable height sampled by the optically trapped particle is,

$$z_p = z_o - \frac{\pi D^3}{6}\frac{(\rho_p - \rho_f)g}{k_s} \tag{14}$$

For a silica particle, $\rho_p - \rho_f \approx 1650 kg/m^3$, and g likely exhibits only a small variation. The parameter z_o scales with laser current and is unlikely to vary significantly between experiments. The spring constant is inversely proportional to diameter and directly proportional to current as discussed above. Hence, particle diameter is the only parameter that explains the presence of large CIs at higher input currents.

To explore how this variation can be observed in our model, we performed additional simulations for two more particle diameters, 1.36 μm and 1.76 μm. These diameters were selected to be consistent with the upper and lower ranges for diameters measured with DLS. The results of these simulations, shown in Fig. 3, illustrate that a lower-than-average particle diameter will result in a higher corner frequency value, while a higher particle diameter results in the opposite trend. In effect, the corner frequency scales as the inverse of particle diameter ($f_c \propto D^{-1}$). This implies that particle polydispersity (i.e., diameter variability) could influence the experimentally observed corner frequency. Based on how corner frequency is connected to the calculation of spring constant and viscosity as discussed in Section 2C, we expect that polydispersity will impact our measurements of these parameters.

The ensemble-averaged spring constant measured at the input currents used in the work are shown in Fig. 4. Based on our experimental results, the spring constant appears to be linearly proportional to input current, with a trend line of $k_s = 4.332 \times 10^{-4} \quad I_{laser} \quad [pN/\mu m]$. The CIs for lower input currents are narrow compared to those observed for 250 mA and 300 mA. As discussed above, this is likely the result of polydispersity. We illustrate this by performing simulations for three different particle diameters: 1.36 μm, 1.56 μm, and 1.76 μm. The ensemble-averaged results for the simulated 1.56 μm diameter particles appears to follow the average value predicted by experiment. However, the simulations show that the smaller diameter, 1.36 μm, results in a higher-than-average spring constant, and the opposite trend is observed for 1.76 μm. The simulations cover a substantial range of the experimental CIs, which suggests polydispersity could be influencing the

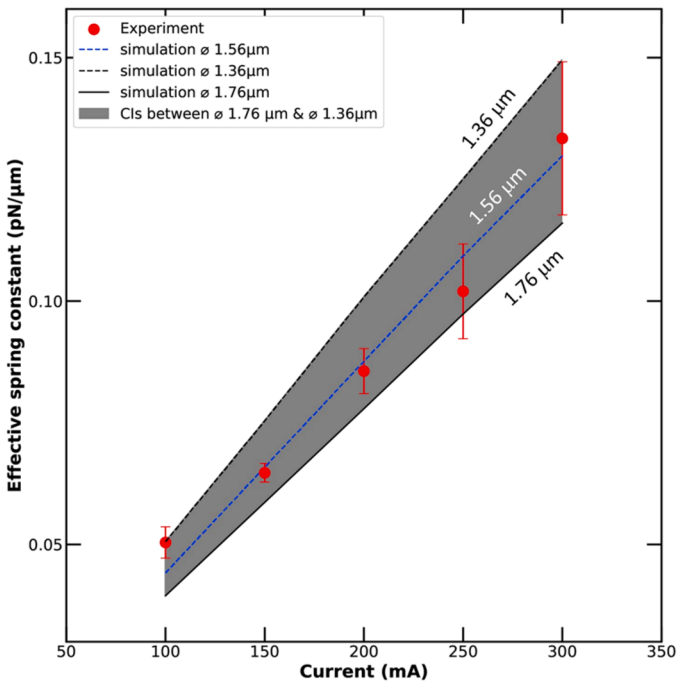

Fig. 4. Data (circles) collected from the ensemble-averaged spring constant for optically trapped particles measured as a function of laser current. Experimental error bars represent 95% CI for N = 10 experiments. Lines show the ensemble-averaged results from 10^5 realizations of 100 simulated particle trajectories for three different particle diameters. A linear fit to experimental data shows that spring constant is approximately $k_s = 4.332 \times 10^{-4} I_{laser}$ $[pN/\mu m]$.

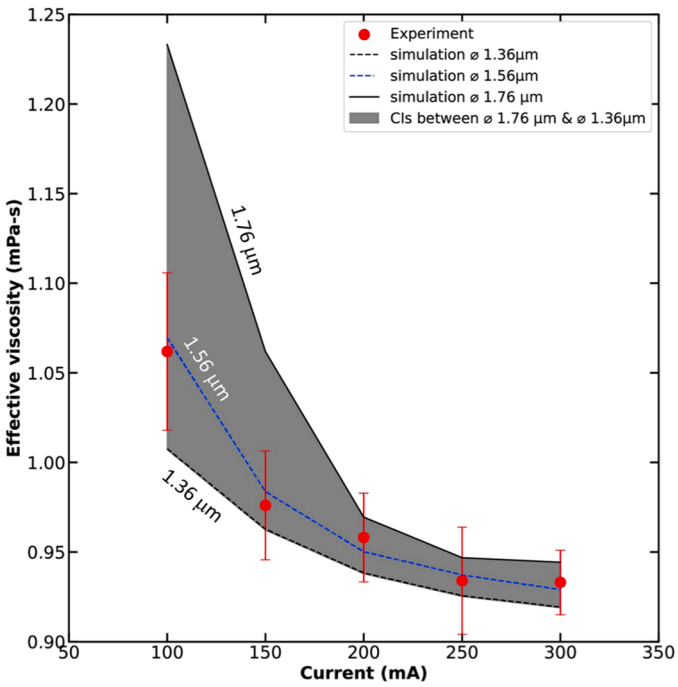

Fig. 5. Data (circles) collected from the ensemble-averaged effective viscosity for optically trapped particles measured as a function of laser current. Experimental error bars represent 95% CI for N = 10 experiments. Lines show the ensemble-averaged results from 10^5 realizations of 100 simulated particle trajectories for three different particle diameters.

results presented here. We also note that, with corner frequency being linearly proportional to spring constant, this effect likely gives rise to the close linear dependence observed in Fig. 3.

Fig. 5 shows the measurement of effective viscosity as a function of input current. We note that the measured viscosity at 100 mA is ~19% higher than the value expected for room temperature water (0.89 mPa-s). The drop in effective viscosity with increasing input current is also observed in simulation. Based on simulations performed at 100 mA, a 1.56 µm diameter particle is held at a most probable position of $z_p \approx 2.6\mu m$. This corresponds to an ensemble average friction factor of $\mu_{eff}/\mu_o \approx 1.19$, which explains the higher-than-expected value for viscosity at lower input currents. The discrepancy diminishes to 4% for 300 mA. We also compare the observed CIs to simulations for 1.36 µm and 1.76 µm diameter particles. The simulations illustrate that a larger diameter particle results in higher effective viscosity measurements, while smaller particles result in smaller effective viscosities. The reason for this effect can be observed when we consider how diameter influences the most probable height of the particle, Eq. 14, which exhibits a diameter cubed (D^3) scaling. The impact can be determined by examining larger particles as an example. In this situation, larger particles will sit at a lower probable height, which also brings the particle in closer proximity to the substrate above which it is optically trapped. This influences the ensemble-averaged friction factor of the particle,

$$\langle f \rangle = \frac{12420\alpha_p^2 + 12233\alpha_p + 431}{12420\alpha_p^2 + 5654\alpha_p + 100} \tag{15}$$

where $\alpha_p = 2z_p/D - 1$. Recalling that the ensembled-averaged friction factor is defined as $\langle f \rangle = \mu_{eff}/\mu_o$, we find that larger particles experience more significant hydrodynamic interactions due to the proximity of the boundary. Hence, the effective viscosity, $\mu_{eff} = \mu_o \langle f \rangle$, manifests itself as an apparently non-Newtonian behavior as a function of laser current, despite the experiment being performed in a Newtonian medium. The hydrodynamic interactions in the experiment can be mitigated by using a high current input for the optical trap, enabling a more accurate measurement of viscosity.

The use of optical trapping as a method for measuring viscosity is significantly impacted by the maximum measurable viscosity. An estimate for this viscosity can be obtained using the scaling model presented by Wirtz in his review of particle tracking microrheology [46],

$\mu_{\max} = \frac{4k_B T\sigma}{3\pi D\varepsilon^2}$ where μ_{max} is the upper viscosity limit that can be measured with optical techniques, σ is the lag time between data points (σ ~1 ms for our experiments), and ε is the smallest measurable fluctuation in our system, also known as static error. To obtain an estimate for ε, we utilize a method by which the particle is exposed to a salt solution [47], which causes the particle to adhere to the boundary. We then recorded eight separate measurements of the stuck particle using our QPD, which we used to construct the mean square displacement (MSD) of the stuck particle in the x and y directions. Based on analyses done by other authors on the issue of measurement limitations [48], the static error, ε, corresponds to the MSD value at the first MSD lag time where $t_{lag} = \sigma$ (see the Supplemental Information for additional details). By this analysis, we obtain an ensemble averaged value of $\varepsilon \approx 3.6nm$ for our measurement system. This estimate for ε limits our measurement to a maximum sample viscosity of ~63 mPa-s. In order to extend this analysis to more viscous materials, we suggest using a smaller diameter. Other authors [49,50] have demonstrated a link between static error and lag time, thus reducing lag time is another possible approach to improving the maximum measurable viscosity.

5. Conclusion

This article presents a model for optical trapping that incorporates particle-wall hydrodynamic interactions. This model is numerically integrated using a midpoint algorithm, with the results from these simulations analyzed to extract dynamical information (e.g., corner frequency, spring constant, and effective viscosity) from particle tra-

jectories. Our simulation results show that hydrodynamic interactions do influence the dynamical properties of optically trapped particles. Our validation experiments show that measured viscosity at 100 mA is ~19% higher than the value expected for room temperature water (0.89 mPa-s). The discrepancy diminishes to 4% when a 300 mA current is used. Simulations performed with the BD model show that, for a nominal spring constant of $k_s = 4.332 \times 10^{-4} I_{laser}$ $[pN/\mu m]$, the discrepancy can be explained via hydrodynamic interactions that influence the measured effective viscosity. Wide variability in CIs observed in our data can be replicated by using a range of diameters in our simulation. This is consistent with DLS measurements of the particles used in this study, which show that the mean diameter was (1.63 ± 0.28) μm. Our simulations show that the CIs fall within a band that encompasses the range of diameters measured using DLS. The measurement presented in this work is limited to a maximum viscosity of ~63 mPa-s, although reducing the trapped particle diameter or measurement lag time could improve this. Overall, this work has implications for optical trapping measurements in Newtonian media. The model presented here may be adapted to address a wide range drag enhancement issues observed in optical trapping experiments. We aim to extend this work examining the impact that hydrodynamic interactions have on optical trapping measurements in non-Newtonian media.

CRediT authorship contribution statement

Richa Ghosh: Conceptualization, Data curation, Formal analysis, Investigation, Methodology, Software, Validation, Visualization, Writing – original draft. **Sarah A. Bentil:** Funding acquisition, Project administration, Resources, Supervision, Writing – review & editing. **Jaime J. Juárez:** Conceptualization, Data curation, Formal analysis, Funding acquisition, Investigation, Methodology, Project administration, Resources, Supervision, Visualization, Writing – review & editing.

Declaration of Competing Interest

The authors declare the following financial interests/personal relationships which may be considered as potential competing interests: Jaime J. Juarez reports financial support was provided by National Science Foundation. If there are other authors, they declare that they have no known competing financial interests or personal relationships that could have appeared to influence the work reported in this paper.

Data availability

Data will be made available on request.

Acknowledgements

This work was performed with the support of National Science Foundation (NSF) funding. JJJ and SAB gratefully acknowledge support from NSF Mechanics of Materials program through award #2114565.

Appendix A. Supporting information

Supplementary data associated with this article can be found in the online version at doi:10.1016/j.colsurfa.2023.132942.

References

[1] G. Pesce, P.H. Jones, O.M. Maragò, G. Volpe, Optical tweezers: theory and practice, Eur. Phys. J. 135 (2020), 949, https://doi.org/10.1140/epjp/s13360-020-00843-5.
[2] B. Landenberger, H. Höfemann, S. Wadle, A. Rohrbach, Microfluidic sorting of arbitrary cells with dynamic optical tweezers, Lab a Chip 12 (2012) 3177–3183, https://doi.org/10.1039/C2LC21099A.
[3] D. Zhang, A. Barbot, B. Lo, G.-Z. Yang, Distributed force control for microrobot manipulation via planar multi-spot optical tweezer, Adv. Opt. Mater. 8 (2020), 2000543, https://doi.org/10.1002/adom.202000543.
[4] M.D. Summers, R.D. Dear, J.M. Taylor, G.A.D. Ritchie, Directed assembly of optically bound matter, Opt. Express, Oe. 20 (2012) 1001–1012, https://doi.org/10.1364/OE.20.001001.
[5] G. Trefalt, T. Palberg, M. Borkovec, Forces between colloidal particles in aqueous solutions containing monovalent and multivalent ions, Curr. Opin. Colloid Interface Sci. 27 (2017) 9–17, https://doi.org/10.1016/j.cocis.2016.09.008.
[6] Y. Deng, J. Bechhoefer, N.R. Forde, Brownian motion in a modulated optical trap, J. Opt. A: Pure Appl. Opt. 9 (2007) S256, https://doi.org/10.1088/1464-4258/9/8/S20.
[7] G.M. Gibson, J. Leach, S. Keen, A.J. Wright, M.J. Padgett, Measuring the accuracy of particle position and force in optical tweezers using high-speed video microscopy, Opt. Express, Oe. 16 (2008) 14561–14570, https://doi.org/10.1364/OE.16.014561.
[8] A. Buosciolo, G. Pesce, A. Sasso, New calibration method for position detector for simultaneous measurements of force constants and local viscosity in optical tweezers, Opt. Commun. 230 (2004) 357–368, https://doi.org/10.1016/j.optcom.2003.11.062.
[9] J. Mo, M.G. Raizen, Highly resolved brownian motion in space and in time, Annu. Rev. Fluid Mech. 51 (2019) 403–428, https://doi.org/10.1146/annurev-fluid-010518-040527.
[10] C. Ha, H.D. Ou-Yang, H.K. Pak, Direct measurements of colloidal hydrodynamics near flat boundaries using oscillating optical tweezers, Phys. A: Stat. Mech. Its Appl. 392 (2013) 3497–3504, https://doi.org/10.1016/j.physa.2013.04.014.
[11] A.J. Goldman, R.G. Cox, H. Brenner, Slow viscous motion of a sphere parallel to a plane Wall.I. Motion through a quiescent fluid, Chem. Eng. Sci. 22 (1967) 637.
[12] S. Ito, N. Toitani, H. Yamauchi, H. Miyasaka, Evaluation of radiation force acting on macromolecules by combination of Brownian dynamics simulation with fluorescence correlation spectroscopy, Phys. Rev. E. 81 (2010), 061402, https://doi.org/10.1103/PhysRevE.81.061402.
[13] Z. Xu, W. Song, K.B. Crozier, Direct particle tracking observation and brownian dynamics simulations of a single nanoparticle optically trapped by a plasmonic nanoaperture, ACS Photonics 5 (2018) 2850–2859, https://doi.org/10.1021/acsphotonics.8b00176.
[14] G. Volpe, G. Volpe, Simulation of a Brownian particle in an optical trap, Am. J. Phys. 81 (2013) 224–230, https://doi.org/10.1119/1.4772632.
[15] M. Pancorbo, M.A. Rubio, P. Domínguez-García, Brownian dynamics simulations to explore experimental microsphere diffusion with optical tweezers, Procedia Comput. Sci. 108 (2017) 166–174, https://doi.org/10.1016/j.procs.2017.05.231.
[16] J. Herranen, J. Markkanen, G. Videen, K. Muinonen, Non-spherical particles in optical tweezers: a numerical solution, PLOS ONE 14 (2019), e0225773, https://doi.org/10.1371/journal.pone.0225773.
[17] W. Vigilante, O. Lopez, J. Fung, Brownian dynamics simulations of sphere clusters in optical tweezers, Opt. Express, Oe. 28 (2020) 36131–36146, https://doi.org/10.1364/OE.409078.
[18] S. Xu, Z. Sun, Computer simulation on the collision-sticking dynamics of two colloidal particles in an optical trap, J. Chem. Phys. 126 (2007), 144903, https://doi.org/10.1063/1.2712183.
[19] G. Qiu, Y. Du, Y. Guo, Y. Meng, Z. Gai, M. Zhang, J. Wang, A. deMello, Plasmofluidic-based near-field optical trapping of dielectric nano-objects using gold nanoislands sensor chips, ACS Appl. Mater. Interfaces 14 (2022) 47409–47419, https://doi.org/10.1021/acsami.2c12651.
[20] R.R. Agayan, R.G. Smith, R. Kopelman, Slipping friction of an optically and magnetically manipulated microsphere rolling at a glass-water interface, J. Appl. Phys. 104 (2008), 054915, https://doi.org/10.1063/1.2976355.
[21] E. Schäffer, S.F. Nørrelykke, J. Howard, Surface forces and drag coefficients of microspheres near a plane surface measured with optical tweezers, Langmuir 23 (2007) 3654–3665, https://doi.org/10.1021/la0622368.
[22] L.C. Geonzon, M. Kobayashi, Y. Adachi, Effect of shear flow on the hydrodynamic drag force of a spherical particle near a wall evaluated using optical tweezers and microfluidics, Soft Matter 17 (2021) 7914–7920, https://doi.org/10.1039/D1SM00876E.
[23] D. Andrén, N. Odebo Länk, H. Šípová-Jungová, S. Jones, P. Johansson, M. Käll, Surface interactions of gold nanoparticles optically trapped against an interface, J. Phys. Chem. C. 123 (2019) 16406–16414, https://doi.org/10.1021/acs.jpcc.9b05438.
[24] S. Zhang, L.J. Gibson, A.B. Stilgoe, T.A. Nieminen, H. Rubinsztein-Dunlop, Impact of complex surfaces on biomicrorheological measurements using optical tweezers, Lab Chip 18 (2018) 315–322, https://doi.org/10.1039/C7LC01176H.
[25] S. Zhang, L.J. Gibson, A.B. Stilgoe, T.A. Nieminen, H. Rubinsztein-Dunlop, Measuring local properties inside a cell-mimicking structure using rotating optical tweezers, J. Biophotonics 12 (2019), e201900022, https://doi.org/10.1002/jbio.201900022.
[26] J. Kim, O.J.F. Martin, Surfactants control optical trapping near a glass wall, J. Phys. Chem. C. 126 (2022) 378–386, https://doi.org/10.1021/acs.jpcc.1c08975.
[27] L.C. Geonzon, M. Kobayashi, T. Sugimoto, Y. Adachi, Study on the kinetics of adsorption of poly(ethylene oxide) onto a silica particle using optical tweezers and microfluidics, Colloids Surf. A: Physicochem. Eng. Asp. 642 (2022), 128691, https://doi.org/10.1016/j.colsurfa.2022.128691.
[28] E.J.G. Peterman, F. Gittes, C.F. Schmidt, Laser-induced heating in optical traps, Biophys. J. 84 (2003) 1308–1316, https://doi.org/10.1016/S0006-3495(03)74946-7.
[29] C. Cole, Thorlabs KPA101 Python Data Logger, (n.d.). https://github.com/coopercole/KPA101-python-datalogger (accessed July 24, 2023).
[30] C. Riesenberg, C.A. Iriarte-Valdez, A. Becker, M. Dienerowitz, A. Heisterkamp, A. Ngezahayo, M.L. Torres-Mapa, Probing ligand-receptor interaction in living cells using force measurements with optical tweezers, Front. Bioeng. Biotechnol. 8

(2020) https://www.frontiersin.org/articles/10.3389/fbioe.2020.598459 (accessed July 24, 2023).
[31] M. Tassieri, F.D. Giudice, E.J. Robertson, N. Jain, B. Fries, R. Wilson, A. Glidle, F. Greco, P.A. Netti, P.L. Maffettone, T. Bicanic, J.M. Cooper, Microrheology with Optical tweezers: measuring the relative viscosity of solutions 'at a glance, Sci. Rep. 5 (2015), 8831, https://doi.org/10.1038/srep08831.
[32] J. Gieseler, J.R. Gomez-Solano, A. Magazzu, I.P. Castillo, L.P. Garcia, M. Gironella-Torrent, X. Viader-Godoy, F. Ritort, G. Pesce, A. Arzola, K. Volke-Sepulveda, G. Volpe, Optical tweezers - from calibration to applications: a tutorial, Adv. Opt. Photonics 13 (2021) 74–241, https://doi.org/10.1364/AOP.394888.
[33] K. Berg-Sørensen, H. Flyvbjerg, Power spectrum analysis for optical tweezers, Rev. Sci. Instrum. 75 (2004) 594–612, https://doi.org/10.1063/1.1645654.
[34] S.L. Eichmann, S.G. Anekal, M.A. Bevan, Electrostatically confined nanoparticle interactions and dynamics, Langmuir 24 (2008) 714–721, https://doi.org/10.1021/la702571z.
[35] M.A. Bevan, D.C. Prieve, Hindered diffusion of colloidal particles very near to a wall: Revisited, J. Chem. Phys. 113 (2000) 1228–1236.
[36] J. Happel, H. Brenner. Low Reynolds number hydrodynamics: with special applications to particulate media, 1983 edition.,, Springer,, The Hague; Boston: Hingham, MA, USA, 2009.
[37] D.S. Sholl, M.K. Fenwick, E. Atman, D.C. Prieve, Brownian dynamics simulation of the motion of a rigid sphere in a viscous fluid very near a wall, J. Chem. Phys. 113 (2000) 9268–9278, https://doi.org/10.1063/1.1320829.
[38] J. Deng, Q. Wei, Y. Wang, Y. Li, Numerical modeling of optical levitation and trapping of the "stuck" particles with a pulsed optical tweezers, Opt. Express 13 (2005) 3673, https://doi.org/10.1364/OPEX.13.003673.
[39] E. Climent, M.R. Maxey, G.E. Karniadakis, Dynamics of self-assembled chaining in magnetorheological fluids, Langmuir 20 (2004) 507–513.
[40] P.S. Grassia, E.J. Hinch, L.C. Nitsche, Computer simulations of Brownian motion of complex systems, J. Fluid Mech. 282 (1995) 373–403, https://doi.org/10.1017/S0022112095000176.
[41] M. Fixman, Simulation of Polymer Dynamics.1. General Theory, J. Chem. Phys. 69 (1978) 1527–1537.
[42] R. Dey, S. Ghosh, A. Kundu, A. Banerjee, Simultaneous random number generation and optical tweezers calibration employing a learning algorithm based on the brownian dynamics of a trapped colloidal particle, Front. Phys. 8 (2021) https://www.frontiersin.org/articles/10.3389/fphy.2020.576948 (accessed August 15, 2023).
[43] N. Malagnino, G. Pesce, A. Sasso, E. Arimondo, Measurements of trapping efficiency and stiffness in optical tweezers, Opt. Commun. 214 (2002) 15–24, https://doi.org/10.1016/S0030-4018(02)02119-3.
[44] A.T. O'Neil, M.J. Padgett, Axial and lateral trapping efficiency of Laguerre–Gaussian modes in inverted optical tweezers, Opt. Commun. 193 (2001) 45–50, https://doi.org/10.1016/S0030-4018(01)01198-1.
[45] Compact Laser Diode Driver with TEC and Mount for Butterfly Packages, (n.d.). https://www.thorlabs.com (accessed August 16, 2023).
[46] D. Wirtz, Particle-tracking microrheology of living cells: principles and applications, Annu. Rev. Biophys. 38 (2009) 301–326, https://doi.org/10.1146/annurev.biophys.050708.133724.
[47] Design and Documentation (OTZ) | Advanced Lab, (n.d.). https://experimentationlab.berkeley.edu/DesignandDocumentationOTZ (accessed November 22, 2023).
[48] S. Shabaniverki, J.J. Juárez, Characterizing gelatin hydrogel viscoelasticity with diffusing colloidal probe microscopy, J. Colloid Interface Sci. 497 (2017) 73–82, https://doi.org/10.1016/j.jcis.2017.02.057.
[49] A. Kowalczyk, C. Oelschlaeger, N. Willenbacher, Tracking errors in 2D multiple particle tracking microrheology, Meas. Sci. Technol. 26 (2015), 015302, https://doi.org/10.1088/0957-0233/26/1/015302.
[50] S. Shabaniverki, A. Alvarez-Valdivia, J.J. Juárez, Portable Imaging Viscometry for Quantitative Complex Fluid Measurements, Experimental Thermal and Fluid Science. 107 (n.d.) 29–37. https://doi.org/10.1016/j.expthermflusci.2019.05.009.